Biochemical Pharmacology 83 (2012) 551–558

Contents lists available at SciVerse ScienceDirect

Biochemical Pharmacology

journal homepage: www.elsevier.com/locate/biochempharm

In vitro drug metabolism by C-terminally truncated human flavin-containing monooxygenase 3

Gianluca Catucci [a], Gianfranco Gilardi [a], Lars Jeuken [b], Sheila J. Sadeghi [a,*]

[a] Department of Life Sciences and Systems Biology, University of Torino, Italy
[b] Institute of Membrane and Systems Biology, University of Leeds, United Kingdom

ARTICLE INFO

Article history:
Received 23 October 2011
Accepted 30 November 2011
Available online 8 December 2011

Keywords:
Flavin-containing monooxygenase
Molecular docking
In vitro expression
Drug metabolism

ABSTRACT

Human flavin-containing monooxygenase 3 (hFMO3) is a microsomal drug-metabolizing monooxygenase that catalyzes the NADPH-dependent oxygenation of a wide range of drugs and xenobiotics which contain a soft-nucleophiles, usually sulfur or nitrogen. As the release from the microsomal membranes can facilitate the *in vitro* experimental determination of drug metabolism by hFMO3, in this work we identified and eliminated the membrane anchoring sequence without affecting the activity of the enzyme and producing a soluble active enzyme. The truncated hFMO3 carrying a C-terminal deletion of 17 amino acids (tr-hFMO3) was expressed and purified from the cytosolic fraction. The tr-hFMO3 proves to be detached from the membrane, properly folded and fully active towards well-known marker substrates such as benzydamine and sulindac sulfide with measured apparent K_m values of 45 ± 8 μM and 25 ± 4 μM, respectively. Its activity was further tested with newly discovered Aurora kinase inhibitors, Tozasertib and Danusertib, and compared to those of the wild type enzyme.

The use of this soluble form of the hFMO3 enzyme as opposed to the usual microsomal preparations is advantageous for *in vitro* drug metabolism studies that are a requirement in the early phases of drug development by pharmaceutical industry.

1. Introduction

The flavin-containing monooxygenases comprise a family of five functional enzymes and are the second most important phase 1 drug-metabolizing enzymes after cytochromes P450 [1,2]. One member of the family, human flavin-containing monooxygenase 3 (hFMO3) is predominantly expressed in the liver where its substrates, generally nitrogen-, sulfur- and phosphorous-containing soft nucleophiles are transformed into more polar and excretable metabolites [3]. Human FMO3 contributes to the metabolism of many drugs such as ranitidine, cimetidine, tamoxifen, clozapine, benzydamine, amphetamine and mutations in its gene sequence have revealed polymorphisms that can cause significant differences in metabolism and lead to disease, one example of which is trimethylaminuria [4–6]. The enzyme is anchored to the smooth endoplasmic reticulum membrane, where its reduced flavin group binds molecular oxygen and is thought to act as a loaded gun ready to perform nucleophilic attack on the substrates [7–9].

To date the three-dimentional structure of hFMO3 has not been solved due to difficulties in the crystallization of microsomal, membrane-bound proteins [10]. In the past, several reports have demonstrated a successful increase in the solubility of membrane proteins by deleting the anchor that binds them to the membranes [11–13]. In 1991 Ozols [14] revealed that the C-terminus of FMO2 is very hydrophobic and it could anchor the protein to the membrane. More recently, Krueger et al. [15] reported on the expression and purification attempts of a soluble rabbit FMO2 by deleting 26 amino acids from the C-terminus region presumed to function as the membrane anchor.

In the present study, based on the hydrophobic nature of the C-terminus of the protein, a truncated hFMO3 was engineered by deleting the C-terminal region at different amino acid positions. The protein sequence with a 17 amino acid deletion (tr-hFMO3) was expressed and purified. The tr-hFMO3 proves to be detached from the membrane and it is not only fully active towards well-known marker substrates such as benzydamine and sulindac sulfide, but also newly discovered Aurora kinase inhibitors such as Tozasertib [16] and Danusertib [17].

The use of this soluble form of the hFMO3 enzyme as opposed to the usual microsomal preparations is advantageous for *in vitro* drug metabolism studies that are a requirement in the early phases of drug development by pharmaceutical industry. These studies are important not only in revealing potential metabolites but also

* Corresponding author at: Department of Life Sciences and Systems Biology, Via Accademia Albertina 13, 10123 Torino, Italy. Tel.: +39 011 6704528; fax: +39 011 6704643.
E-mail address: sheila.sadeghi@unito.it (S.J. Sadeghi).

0006-2952/$ – see front matter © 2011 Published by Elsevier Inc.
doi:10.1016/j.bcp.2011.11.029

allowing for elucidation of their toxicity and any possible adverse drug reactions.

2. Experimental procedures

2.1. Reagents

Methimazole (MMI), sulindac, sulindac sulfide, benzydamine, benzydamine N-oxide, FAD, Igepal, acetronitrile, methanol, NADPH and 5,5′-dithiobis(2-nitrobenzoate) and salts were purchased from Sigma–Aldrich (Italy). Tozasertib and Danusertib were purchased from Aurogene (Italy).

2.2. Molecular dynamics

Molecular dynamics in membrane was done using the YASARA [18] "md run membrane" for 4 ns. YASARA automatically identified the C-terminus of the hFMO3 as a hydrophobic exposed region bound to the membrane and constructed a membrane environment accordingly. YASARA unequivocally assigned the sequence between residues ARG 504 and THR 532 to a putative transmembrane helix and the protein was automatically rotated in order to fill the simulation cell volume with physiological solution and lipid content accordingly to the C-terminal helix. For all simulations, AMBER 03 force field was applied.

2.3. Protein–ligand interaction study

AutoDock 4.0 [19], embedded into the YASARA Structure package, was used to dock benzydamine, sulindac sulfide, tozasertib and danusertib to the refined model. Danusertib and tozasertib were obtained from the HIC-UP [20] database for hetero-compounds and were utilized with the same coordinates as they can be found in the co-crystals with the kinase domain of Abl [21] and Aurora kinase AurA [22], respectively. Benzydamine and sulindac sulfide were obtained from PubChem (www.ncbi.nlm.nih.gov/pccompound) and were geometrically optimized using MOPAC [23] also embedded in the YASARA package. The optimized ligand molecules were docked into the refined protein model by running twenty-five of Global Docking centering a $15 \times 15 \times 15$ Å simulation cell on the FAD group. In YASARA, docking runs of the ligand to receptor yield results sorted by binding energy where more positive energies indicate stronger binding and negative energies equate to no binding. After global docking the best binding mode (pose) was selected based on the best binding energy. The complexes were then subjected to 999 runs of Local Docking yielding the final docked binding modes.

The global docking experiment, in which the drug is originally outside the simulation box and is placed inside the cell by exploiting the autodock algorithm, resulted in a series of binding modes classified by the binding energy outputs. Among these binding modes the complex protein-ligand bearing the highest binding energy calculated by YASARA [18] as the mechanical energy required for disassembling a whole into separate parts, was selected and refined by local docking. In local docking experiments the ligand is within the simulation cell and the possible conformations are assayed for a maximum of 999 runs and the results are again sorted by binding energy. In this case, since the starting positions of the ligand inside the simulation box are often random and it is probable that a certain pose/binding mode could never be detected, molecular dynamics simulations were applied to better accommodate the ligand inside the pocket.

2.4. Cloning, expression and purification

WT hFMO3 was cloned in the expression vector pJL2 [24] using the two restriction enzymes XbaI and HindIII previously [25]. The plasmid was digested by these two enzymes and the gene was amplified with the primers: 5′ AGT TCC CAG AAC TCT AGA ATG GGG AAG AAA GTG GCC ATC 3′ as forward for all the reactions, 5′ GCT CAT CGA AGC TTT TAA TGG TGA TGG TGC CGG TCC CAC TGG GTC AGT AT 3′ as a reverse for 493X, 5′ GCT CAT CGA AGC TTT TAA TGG TGA TGG TGT CTC CCG ACC ACT CGT GTC TG 3′ as a reverse for 505X and 5′ GCT CAT ATA AGC TTT TAA TGG TGA TGG TGC AGC CAA TGG AAA AAG AAG CAA GGC 3′ as a reverse for 516X (tr-hFMO3). All the reverse primers contained the sequence coding for a 4His-tag (5′ ATGGTGATGGTG 3′), to assist in the purification. The amplified genes were then digested with the restriction enzymes XbaI and HindIII and cloned back into pJL2.

Wild type and the tr-hFMO3 were expressed in *E. coli* JM109 cells and grown 24 h post-induction. WT protein was purified from the membrane fractions whereas the truncated hFMO3 was purified from the cytosolic fraction. All other purification steps were identical. Both proteins were purified via Ni affinity chromatography. Spectra of the eluted fractions (with 40 mM histidine) were recorded using a diode array HP-8453E spectrophotometer. FAD containing fractions with the characteristic absorption peaks at 375 and 442 nm were pooled and exchanged to storage buffer (100 mM potassium phosphate buffer pH 7.4, 20% glycerol and 1 mM EDTA) by 30 kDa cutoff Amicon membranes and stored at −20 °C.

2.5. FAD content determination

The concentration of holo hFMO3 was determined by spectroscopy with the peak absorbance at 450 nm and an extinction coefficient of 11,900 M^{-1} cm^{-1}, as previously described for other flavin-containing enzymes [26]. This value was also used for the determination of the enzyme concentration under non-denaturing conditions. In addition to the active enzyme (flavin-bound) concentration, the total hFMO3 protein concentration for the final purified protein was determined using both absorbance at 280 nm (extinction coefficients of 87,520 M^{-1} cm^{-1} and 87,485 M^{-1} cm^{-1} for WT and tr-hFMO3, respectively) and Bradford assay.

2.6. Far-UV circular dichroism analysis

Far UV circular dichroism experiments were performed on the WT and tr-hFMO3 at room temperature (Jasco-J600 spectropolarimeter). In order to improve the signal-to-noise ratio, several (3–4) spectra were accumulated and averaged for each sample. The measurements were carried out using 5 μM of protein and quartz cuvettes with a path length of 0.1 cm for the far UV (200–250 nm). Secondary structure prediction for both enzymes was performed using the K2D2 algorithm [27].

2.7. FAD aerobic reduction

The protein was diluted to 7 μM in 50 mM potassium phosphate buffer pH 7.4 at 10 °C. After the addition of aerated NADPH spectra were recorded using a Hewlett-Packard diode array spectrophotometer. The re-oxidation of the enzyme was followed by measuring the increase in absorbance at 442 nm.

2.8. Enzyme-substrate incubations and HPLC analysis

WT and tr-hFMO3 catalyzed S-oxygenation of MMI was monitored using the method previously described [28,29] at 37 °C. Rates of N-oxygenation of benzydamine [30] and

S-oxygenation of sulindac sulfide [31] for WT and tr-hFMO3 were determined using HPLC methods described previously. A typical incubation mixture consisted of 50 mM potassium phosphate buffer (pH 7.4), NADPH, the substrate and 0.17 μM of purified enzyme in a final volume of 0.20 ml. Incubations were carried out at 37 °C for 10 min: the linearity of product formation was confirmed with purified hFMO3 preparations for 20 min. The reaction was terminated by the addition of 0.10 ml of ice-cold acetonitrile for benzydamine and by adding 50 μL of 50% phosphoric acid and 1.0 ml of ethyl acetate for sulindac sulfide. For sulindac sulfide, after centrifugation at 2000 × *g* for 10 min, the organic phase was transferred to a clean tube and evaporated in a vacuum pump. The residue was dissolved in 0.20 ml of mobile phase (50% acetonitrile in 25 mM potassium phosphate buffer, pH 3.0) and introduced into the HPLC apparatus (Agilent-1200 series). For benzydamine the aqueous supernatant was centrifuged at 2000 × *g* for 10 min and was subjected to HPLC equipped with a 4.6 × 150 mm 5 μm Eclipse XDB-C18 column at room temperature and the UV–visible detector was set at 308 nm. A sample of 20 μl was injected and the separation was performed using a mobile phase of 32% acetonitrile and 68% 50 mM KH_2PO_4 pH 7.4 at a flow rate of 1.4 ml/min, which was increased to 1.8 ml/min after 7 min. The formation of sulindac sulfoxide was monitored at 360 nm [31]. The kinetic analysis of N or S-oxygenation was carried out using a nonlinear regression analysis program (SigmaPlot).

In the case of hFMO3-catalyzed N-oxygenation of tozasertib and danusertib, a typical incubation mixture consisted of 50 mM potassium phosphate buffer (pH 7.4), NADPH, the substrate and 0.17 μM of purified enzyme in a final volume of 0.20 ml. Incubations were carried out at 37 °C for 10 min: the linearity of product formation was confirmed with purified hFMO3 preparations for 20 min. The incubation was terminated by the addition of 0.10 ml of ice-cold methanol. The aqueous supernatant was centrifuged at 2000 × *g* for 10 min and was subjected to HPLC equipped with an analytical C18 column (4.6 × 150 mm, 5 μm). A 75 μl sample was injected and the separation was performed using a mobile phase of 70% methanol and 30% water at a flow rate of 1.0 ml/min. The formation of tozasertib N-oxide was monitored at the wavelength of 250 nm while the danusertib N-oxide product was monitored at 295 nm.

2.9. Enzyme interaction with the lipid bilayer (QCM-D)

Small Unilaminar Vesicles (SUV) were formed by tip sonicating EggPC (5 mg/ml, Avanti Lipids) in MOPS buffer (20 mM MOPS pH 7.4, 30 mM Na_2SO_4) for 30 min at 4 °C until clear. Tip particles were removed by spinning the sample for 5 min at 14,500 × *g*. SUVs were stored at 4 °C and used within two days. Directly before the experiment, the sample was diluted to 0.5 mg/ml in Milli-Q water (18.2 MΩ cm^2).

SiO_2-coated crystals (Q-sense) were bath sonicated in 0.4% SDS (Sigma) for 30 min, followed by sonication in Milli-Q for another 30 min. The crystals were then further treated for 30 min with UV/ozone (UV/ozone cleaning system, low pressure quartz-mercury vapor lamp emitting 254 and 185 nm UV, UVOCS, Montgomeryville) and installed in the Quartz-Crystal Microbalance with Dissipation (QCM-D) equipment (Q-Sense E4, Q-Sense AB, Gothenburg, Sweden). After equilibrating the crystals with buffer (all experiments were performed with a flow rate of 70 μL/min), they were incubated with the EggPC SUV (0.5 mg/ml) until a stable response was observed (typically 10 min), indicating that a planar solid-supported bilayer is formed. The QCM-D crystals were then rinsed with Milli-Q water, followed by MOPS buffer. Finally, the crystals were incubated with 1 μM hFMO3 and tr-hFMO3 in MOPS buffer. Human FMO3 was made up from a 100 μM stock solution containing 0.1% (v/v) of the detergent, Igepal, thus reducing the Igepal to about 0.001% (v/v). Control experiments were performed to check that these levels of detergent in the hFMO3 sample do not disrupt the sBLM and no effect was observed for Igepal up to 0.005% (v/v).

3. Results

3.1. Membrane anchoring and construction of the truncated hFMO3

In order to facilitate the *in vitro* experimental determination of drug metabolism by hFMO3 we identified and eliminated its membrane anchor producing a soluble and active enzyme. It has previously been hypothesized that the C-terminal region of hFMO3 is responsible for its anchoring to the membrane [9,14], therefore we analysed the primary sequence of this enzyme and the resulting hydropathy plot (Fig. 1) pointed to a putative transmembrane region starting from resdiue 516 in the C-terminus of this protein. In addition to the hydropathy plot, *in silico* molecular dynamics experiments were also carried out (data not shown) which also demonstrated the presence of a putative transmembrane helix consisting of amino acid residues between 504 and 532 in the C-terminus.

Based on the above-mentioned analyses, a series of C-terminus truncated hFMO3 sequences were generated and cloned in the expression vector pJL2. The purpose of the truncation was to interrupt the hFMO3 gene at the level of the C-terminal region of the protein and to obtain a more soluble enzyme with less affinity to the hydrophobic membrane. Three truncated constructs were engineered by introducing a stop codon in the hFMO3 gene at positions codifying for ARG 492, LYS 505 and LYS 516. Due to the higher expression level of the construct called tr-hFMO3 corresponding to the protein with the least number of amino acid deletions (i.e. stop codon at LYS 516), only this protein was closed for the subsequent *in vitro* characterisation experiments.

3.2. Purification and spectroscopical characterisation of the truncated hFMO3

Wild type hFMO3 was heterologously expressed in *E. coli* and purified to serve as a control for the truncation experiments. Two

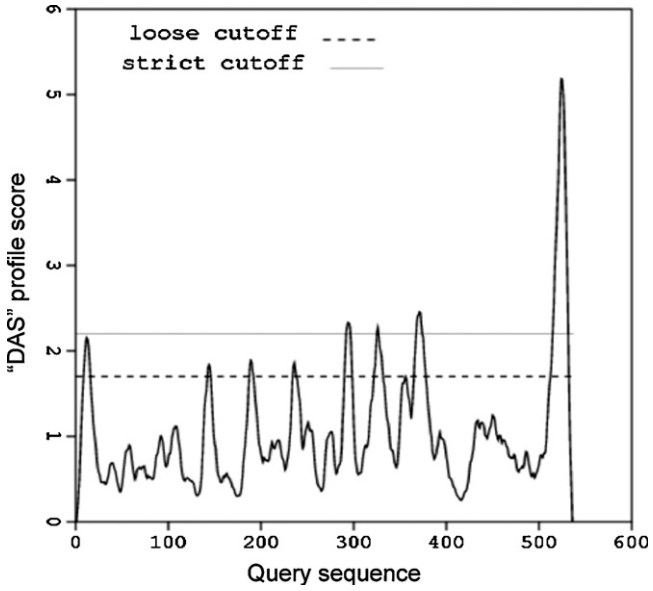

Fig. 1. Hydropathy Plot: the hFMO3 primary sequence was used to predict local hydrophobic patches using the DAS-TM plot: a clear hydrophobic sequence is shown at the C-terminus.

ultra-centrifugations steps were required for the wild type protein, prior to loading the membrane fraction onto a DEAE ion exchange chromatography that cleared the bacterial crude extract, not retaining hFMO3 at pH 7.4. This was followed by a Ni-affinity column that led to a pure protein. On the other hand, the tr-hFMO3 required only one ultra-centrifugation step that gave a supernatant corresponding to the cytosolic fraction containing the protein that was ready for the subsequent DEAE and Ni chromatography steps described above. The yield of pure protein was determined using the absorbance of the aromatic residues at 280 nm in combination with the Bradford protein assay, leading to approximately 12–13 mg per litre of culture in case of the WT protein and 9–10 mg per litre of culture for the truncated form. SDS–PAGE analysis of the Ni-affinity purified samples showed a band at approximately 60 kDa (Fig. 2A) in good agreement with the molecular weight calculated from the amino acid sequence of hFMO3.

Both purified WT and tr-hFMO3 exhibited a yellow colour typical of FAD. The elution profile showed a clear correlation between the total protein content and the FAD absorbance at 450 nm. The FAD content of the purified proteins (holoprotein-determined by absorbance at 450 nm) was compared to the total hFMO3 concentration (holo and apoprotein-determined at 280 nm). The molar ratios showed 85% and 91% of holo-protein content for WT and tr-hFMO3, respectively.

The purified proteins were further characterised by spectroscopy. In the first instance, reduction of the WT and tr-hFMO3 were carried out aerobically in the presence of NADPH (in the absence of the substrate) that rapidly bleaches the protein solutions. Fig. 2C and D shows the oxidised spectra for wild type and tr-hFMO3 with the maxima at 372 and 442 nm together with the reduced forms. As it can be seen in the figure, the truncation has had no effect on the NADPH binding and subsequent reduction of the protein.

In order to confirm that the truncation of the C-terminus of hFMO3 did not affect the overall folding of the protein, the far-UV CD spectra of tr-hFMO3 were recorded and compared to those of the wild type protein. Fig. 2B shows the overlapped far UV CD spectra of WT and tr-hFMO3. As it can be seen, the structure of tr-hFMO3 has a reduced helical content as verified by the lower CD intensity of the two peaks at 208 and 222 nm, and this is ascribed to the C-terminal helix responsible for membrane binding in the wild type. The deletion of the last 17 amino acids of the protein sequence has not compromised the overall secondary structure of the enzyme, as shown by analysis of the far-UV CD spectra with the K2D2 software [27] that led to the results shown in Table 1 showing that both proteins have a predominantly α-helical secondary structure and as expected a 4% reduction in the alpha helices present in tr-hFMO3.

Table 1
Secondary structure content calculated from the far-uv CD spectra analysed by K2D2 software.

Protein	Alpha helices	Beta strands	Random coils	Square distance	Max error
hFMO3	41%	17%	42%	32.2	0.08
tr-hFMO3	37%	20%	43%	29.8	0.08

The fact that tr-hFMO3 was found in the cytosolic rather than in the membrane fraction suggests that this truncated protein has lost the ability to interact with the lipid bilayer. Solid-supported bilayer lipid membranes (sBLM) are very useful in studying the interaction of a protein with model membranes, as protein adsorption and interaction can be followed with Quartz-Crystal Microbalance with Dissipation (QCM-D) measurements. After the formation of a sBLM, the typical QCM-D signal was observed due to the mass of the lipid membrane which changes the QCM-D frequency with −24 Hz and without changing the energy dissipation [32]. Upon addition of 1 μM tr-hFMO3, a sub-monolayer (<1/3 of a full monolayer) adsorbs on the lipid bilayer, which detaches again after rinsing the crystal with buffer (Fig. 3, phase 3, bottom graph). This confirms that tr-hFMO3 has retained little or no affinity for lipid bilayer.

On the other hand, addition of the full-length WT hFMO3 resulted in a rapid decrease in frequency, indicating an increase in mass and thus a strong interaction between the sBLM and WT hFMO3 (Fig. 3, phase 2, top graph). However, this was immediately followed by a loss of material from the surface. We ascribe this

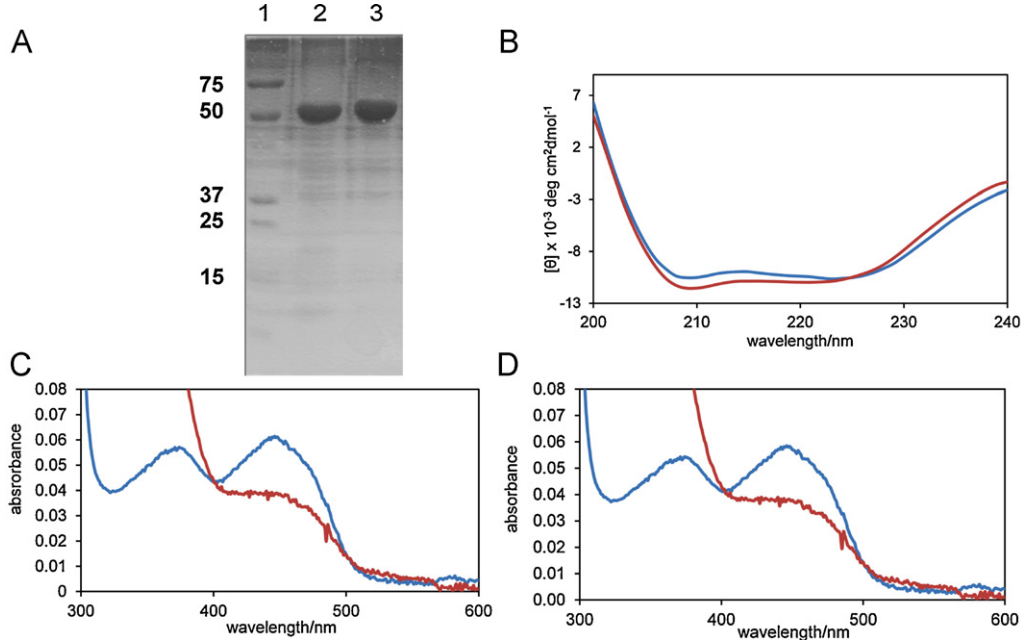

Fig. 2. (A) 10% SDS-PAGE gel of purified hFMO3: Lane 1 shows the molecular weight markers, Lane 2 and 3 truncated and WT hFMO3, respectively (B) Far-UV circular dichroism spectra of the WT hFMO3 (blue) and tr-hFMO3 (red) (C) Aerobic reduction of 5 μM WT hFMO3 and (D) tr-hFMO3 in the presence of equimolar amounts of NADPH. (For interpretation of the references to color in figure legend, the reader is referred to the web version of the article.)

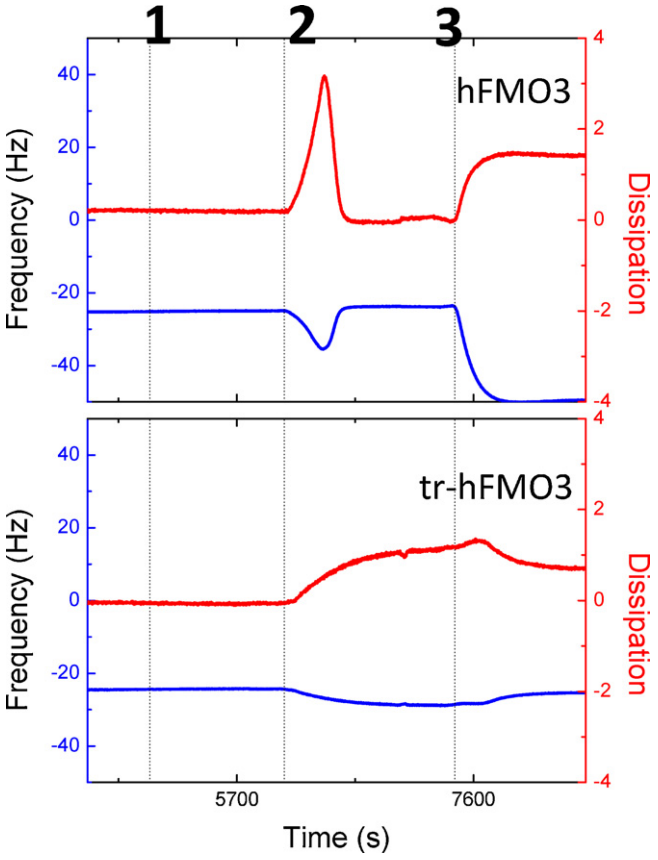

Fig. 3. Quartz crystal microbalance-with dissipation (QCM-D) of the bilayer lipid membranes (sBLM) before (1) and after addition of hFMO3 (top) and tr-hFMO3 (bottom) (2) and subsequent rinsing (3). The data show the decreased ability of tr-hFMO3 to interact with the membrane.

behaviour to the ability of hFMO3 to strip the sBLM off the surface. This hypothesis was confirmed by fluorescent microscopy using fluorescently labelled lipids, which showed that addition of hFMO3 resulted in the destruction of the sBLM and formation of lipid vesicles and aggregates loosely associated with the SiO_2 surface. Interestingly, when the surface was rinsed with buffer (Fig. 3, phase 3), the loosely bound lipid material reabsorbed on the surface and the large increase in mass suggested that a significant amount of hFMO3 co-immobilised on the surface. Fluorescent microscopy confirmed that a partial fluid sBLM is formed after rinsing the surface with buffer (data not shown).

QCM-D provides information regarding the adsorption kinetics and relative mass uptake, and additionally, the dissipation reveals intermediate stages of vesicle adsorption [33]. Fig. 3B shows how QCM-D responses of sBLMs are different after the addition of the WT or tr-hFMO3 enzymes. Both frequency and dissipation signals display a different attitude: WT determines a net change after absorption indicating a strong interaction between the enzyme and the membrane while tr-hFMO3 does not change either frequency or dissipation.

3.3. Metabolism of drugs by the truncated hFMO3

Further characterisation of the tr-hFMO3 included measuring its monooxygenation activity and comparing it to the WT enzyme. For this reason the oxidation of methimazole, benzydamine and suldinac sulfide were investigated. K_m and V_{max} data obtained for tr-hFMO3 are reported in Table 2 where the values are compared with those measured for WT hFMO3. Apparent K_m values for WT and tr-hFMO3 for benzydamine N-oxygenation were 56 ± 8 μM and 45 ± 8 μM respectively, while apparent V_{max} values of 9 for WT and 11 for tr-hFMO3 were obtained. Similar results were obtained using sulindac sulfide S-oxygenation as a marker reaction catalyzed by WT and tr-hFMO3 with K_m values of 25 ± 7 μM and 25 ± 4 μM, respectively. The K_m values obtained for both these known substrates are similar to previously published data using microsomal hFMO3 preparations [34–36].

In all cases the kinetic values measured show that the tr-hFMO3 is not only fully active but also has the same activity range as those measured for the WT protein.

The kinetic characterisation of the tr-hFMO3 was taken one step further by looking at the identity of the products formed by the turnover of the known substrates (drugs) of this enzyme. After each set of reactions at 37 °C in the presence of NADPH, the product(s) was separated by HPLC and the data obtained are shown in Fig. 4A–F. As can be seen from the latter figure, the expected benzydamine N-oxide and suldinac were detected with retention times of 4.0 min and 5.2 min, respectively.

The activity of the tr-hFMO3 enzyme was also tested on tozasertib and danusertib that are involved in cancer treatment as Aurora kinase inhibitors and for which no data on recombinant hFMO3 turnover is available to date. Again in this case the product(s) were separated using HPLC and the data are shown in Fig. 4G–N. The results show that both WT and tr-hFMO3 are able to metabolize these two drugs since extra peaks are observed in the HPLC chromatograms with shorter retention times of 4.1 min for "tozasertib N-oxide" and 3.7 min for "danusertib N-oxide" [37,38].

However, chemical standards for N-oxides of tozasertib and danusertib are not commercially available and in order to ascertain the identity of the products seen in Fig. 4 (H–I–M–N) further characterisation was carried out using LC–MS. The fragmentation of the reaction products of tozasertib and danusertib corresponded to those obtained by Ballard et al. [37] and Cohen's group [38] respectively, confirming that the products were N-oxides of the two kinase inhibitors.

Overall, the data presented demonstrate that the reactions carried out by the tr-hFMO3 are the same as those performed by the WT enzyme.

3.4. Molecular docking

For enzymes where currently the three-dimentional crystal structure is unavailable, molecular modelling studies can enable the development of models that allow predictions of new substrates and design of modulators of enzyme function. To this end, a molecular model of hFMO3 was constructed using the crystal structures of FMO proteins from *Methylophaga* sp. Strain SK1 (PDB: 2VQ7) [39] and *Schizosaccharomyces pombe* (PDB:2GV8)

Table 2
Kinetic parameters of hFMO3 and tr-hFMO3.

	Methimazole			Benzydamine			Sulindac sulfide		
	K_m (μM)	V_{max} (min^{-1})	V_{max}/K_m	K_m (μM)	V_{max} (min^{-1})	V_{max}/K_m	K_m (μM)	V_{max} (min^{-1})	V_{max}/K_m
hFMO3	33 ± 4	71 ± 9	2.2	56 ± 8	9 ± 2	0.2	25 ± 7	108 ± 18	4.3
tr-Hfmo3	35 ± 6	69 ± 12	2.0	45 ± 8	15 ± 7	0.3	22 ± 4	99 ± 21	4.5

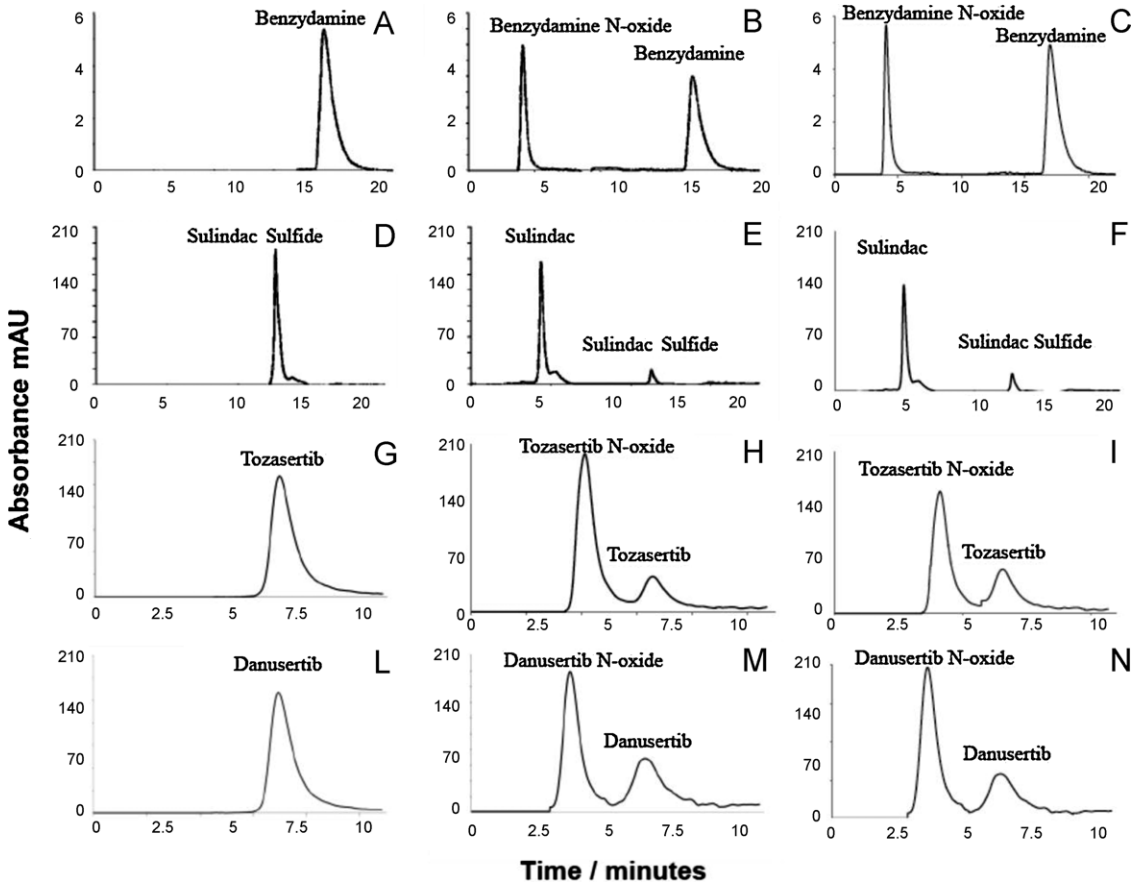

Fig. 4. HPLC chromatograms of incubations of benzydamine, sulindac sulfide, tozasertib and danusertib in the absence (A, D, G, L) and presence of tr-hFMO3 (B, E, H, M) and WT hFMO3 (C, F, I, N) enzymes.

[40] together with a Baeyer–villiger monooxygenase from *Thermobifida fusca* (PDB:1W4X) [41].

As previously hypothesized [9], hFMO3 is thought to act as a loaded gun where the FAD is reduced by NADPH and it is ready to oxygenate any N, S or P containing soft nucleophiles. This mechanism is crucial for the understanding of the active site architecture of the enzyme and the key role exerted by NADPH in catalysis and stabilization. For this reason all docking experiments were carried out in the presence of $NADP^+$ by placing the simulation cell around the isoalloxazinic ring of FAD including all the residues located on the broad substrate exposed cavity of hFMO3 predicted by molecular modelling.

In order to confirm the feasibility of using our 3D generated model for predictions of new substrates of hFMO3, initially docking experiments were performed with the two well-characterised substrates benzydamine and sulindac sulfide, the former N-oxidized and the latter S-oxidized by hFMO3, for which *in vitro* catalysis data were already reported in the previous section.

Docking of benzydamine (an anti-inflammatory drug) and Sulindac sulfide (a non-steroidal anti-inflammatory drug) resulted in complexes with binding energies of 8.46 kcal/mol and 8.90 kcal/mol, respectively. As can be seen from Fig. 5A–B residues LYS 64, ASN 194 and LEU 375 are responsible for the stabilization of both these substrates inside the hFMO3 active site. All these residues interact with the ligands by giving CH/π interactions. As expected the known N-oxidation site of benzydamine is located at the aliphatic chain of this tertiary amine at a distance of 3.5 Å from the C4 of the FAD isoalloxazine ring (Fig. 5A). As for the S-oxidation site of the sulindac sulfide, a similar distance of 3.4 Å from the C4 of the isoalloxazine ring was measured (Fig. 4B).

Both known substrates of hFMO3, benzydamine and sulindac sulfide, interact correctly with its active site by not only resulting in a complex that is energetically favoured, but also by interacting with the enzyme in the expected binding mode for catalysis. These results give strength to our 3D generated model and therefore in a subsequent round of docking simulations the two Aurora kinase inhibitors involved in cancer treatment namely tozasertib and danusertib were tested.

Docking results showed stronger binding energies for both kinase inhibitors compared to those calculated for the known substrates: 9.83 kcal/mol and 11.02 kcal/mol for tozasertib and danusertib, respectively. Fig. 5C–D shows how residues LYS 64, GLU 65, MET 67/MET 66 and ASN 194 are responsible for the stabilization of these kinase inhibitors inside the active site of hFMO3. All these residues interact with both substrates by giving CH/π interactions and the putative N-oxidation sites are at a distance of 3.1 Å for tozasertib and 2.7 Å for danusertib from the C4 of the isoalloxazine ring. In the case of danusertib an extra residue, TYR 462, is involved in the binding mode shown in Fig. 4D. The latter residue interacts with the ligand through π/π interactions leading to the highest calculated binding energy amongst the four drugs tested.

In all the docking experiments reported above, distances of <4 Å between N or S oxidation sites of the substrates and the C4 of the FAD isoalloxazine ring were measured. As mentioned earlier, in these experiments the oxidised structure of FAD was used due to the fact the reduced C4a-hydroperoxyflavin intermediate of FMO enzymes has never been characterised by crystallography and therefore not present in the Protein Data Bank. However, such an intermediate has been observed by single-crystal spectroscopic

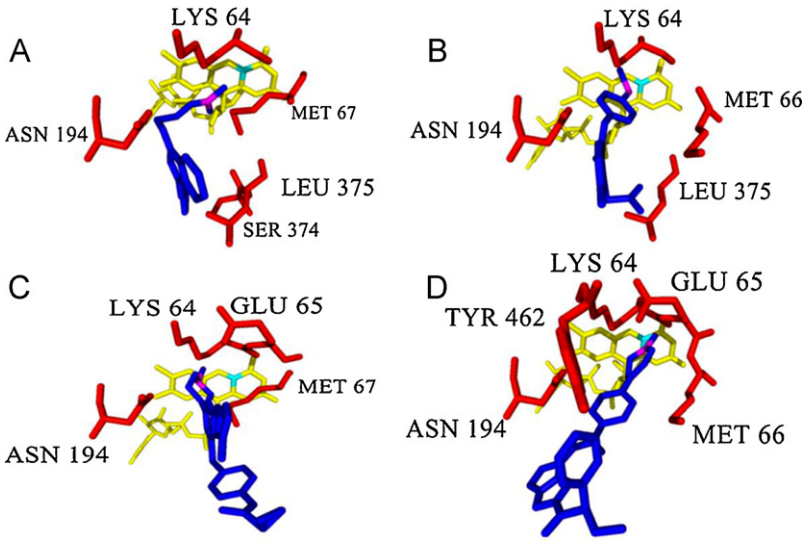

Fig. 5. Docked substrates into the active site of hFMO3 model. FAD is shown in yellow and the substrates are in dark blue. The S or N nucleophilic attack sites of the substrates are shown in magenta with the C4 of the FAD isoalloxazine ring in cyan. Residues interacting with the substrates are shown in red. Benzydamine (A), Sulindac (B), Tozasertib (C) and Danusertib (D). (For interpretation of the references to color in figure legend, the reader is referred to the web version of the article.)

methods and 1.86 Å resolution X-ray crystal structure in the bacterial Choline oxidase, a flavoprotein [42]. Density functional theory calculations carried out for the intermediate seen in Choline oxidase led to measured distance of 3.7 Å (between the oxygen atom of the C4a–OO(H) and the ligand) that is very similar to the distances measured in the docking experiments reported here.

All in all the docking experiments yielded a series of binding modes for each of the docked substrates that were consistent with the correct binding mode of these molecules in the active site of hFMO3 compatible with the nature of the product formed: the nitrogen or the sulfur atom that is the site of the catalysis is not only facing the FAD isoalloxazine ring but it is also within acceptable distance (<4 Å) from the FAD reactive site involved in monooxygenation. These results give strength to the 3D generated model that can be further used for screening of other "probable" substrates of this enzyme.

4. Concluding remarks

To improve the efficiency of drug development by pharmaceutical companies many of them carry out *in vitro* drug metabolism studies using purified enzymes. In the case of hFMO enzymes these studies are currently preformed with microsomal suspensions. In this work we have shown that it is possible to engineer and purify a truncated version of hFMO3 enzyme that has the same catalytic properties of that of the wild type enzyme with added advantage of being also more soluble.

The hydropathy plot of the amino acid sequence of hFMO3 identified the C-terminus as a membrane bound helix. On this basis, a truncated form of hFMO3 was engineered and purified from the cytosolic fraction. Spectroscopic characterisation and secondary structural measurements together with kinetic assays indicate that tr-hFMO3 is very similar to the full-length WT enzyme. Moreover, molecular dynamics in the membrane and QCM-D experiments showed that tr-hFMO3 has a decreased affinity for lipid membranes. These data confirm the role of the C-terminus of hFMO3 in membrane binding and suggest that deletion of the helix does not affect folding, stability and catalytic properties of the enzyme.

A 3D model of hFMO3 was also generated and docking experiments with both known and probable substrates of this enzyme, namely, benzyamine, sulindac sulfide, tozasertib and danusertib were carried out. *In vitro* catalysis experiments of the wild type protein with tozasertib and danusertib confirmed the docking results giving further strength to the model that can be used in the future for screening of other candidate substrates of this enzyme.

Acknowledgements

The authors thank Prof. Maffei (University of Torino) and Mr. Occhipinti for assistance with the mass spectrometry experiments.

References

[1] Cashman JR, Zhang J. Human flavin-containing monooxygenase. Annu Rev Pharmacol Toxicol 2006;46:65–100.
[2] Krueger SK, Williams DE. Mammalian flavin-containing monooxygenase: structure/function, genetic polymorphism and role in drug metabolism. Pharmacol Ther 2005;106:357–87.
[3] Cashman JR. Curr. Human flavin-containing monooxygenase: substrate specificity and role in drug metabolism. Drug Metab 2000;1:181–91.
[4] Kang JH, Chung WG, Lee KH, Park CS, Kang JS, Shin IC, et al. Phenotypes of flavin-containing monooxygenase activity determined by ranitidine N-oxidation are positively correlated with genotypes of linked FMO3 gene mutations in a Korean population. Pharmacogenetics 2000;10:67–78.
[5] Koukouritaki SB, Hines. Flavin-containing monooxygenase genetic polymorphism: impact on chemical metabolism and drug development R.N. Pharmacogenomics 2005;6:807–22.
[6] Reddy RR, Ralph EC, Motika MS, Zhang J, Cashman JR. Drug Metab Dispos 2010;38:2239–45.
[7] Ziegler DM. Recent studies on the structure and function of multi-substrate flavin-containing monooxygenases. Annu Rev Pharmacol Toxicol 1993;33:179–99.
[8] Cashman JR. Structural and catalytic properties of the mammalian flavin-containing monooxygenase. Chem Res Toxicol 1995;8:165–81.
[9] Ziegler DM. An overview of the mechanism, substrate specificities, and structure of FMOs. Drug Metab Rev 2002;34:503–11.
[10] Lee JK, Stroud RM. Unlocking the eukaryotic membrane protein structural proteome. Curr Opin Struct Biol 2010;20:464–70.
[11] Schoch GA, Yano JK, Wester MR, Griffin KJ, Stout CD, Johnson EF. Structure of human microsomal cytochrome P4502C8 – evidence for a peripheral fatty acid binding site. J Biol Chem 2004;279:9497–503.
[12] Ekroos M, Sjogren T. Structural basis for ligand promiscuity in cytochrome P450 3A4. Proc Natl Acad Sci USA 2006;103:13682.
[13] Sansen S, Yano JK, Reynald RL, Schoch GA, Griffin KJ, Stout CD, Johnson EF. Adaptations for the oxidation of polycyclic aromatic hydrocarbons exhibited by the structure of human P450 1A2. J Biol Chem 2007;282:14348–55.
[14] Ozols J. Multiple forms of liver microsomal FMO- complete covalent structure of form-2. Arch Biochem Biophys 1991;290:103–15.
[15] Krueger SK, Vandyke JE, Williams DE, Hines RN. C-terminal truncation of rabbit flavin-containing monooxygenase isoform 2 enhances solubility. Arch Biochem Biophys 2006;450:149–56.

[16] Harrington EA, Bebbington D, Moore J, Rasmussen RK, Ajose-Adeogun AO, Nakayama T, et al. VX-680, a potent and selective small-molecule inhibitor of the Aurora kinases, suppresses tumor growth in vivo. Nature Med 2004;10: 262–7.
[17] Carpinelli P, Ceruti R, Giorgini ML, Cappella P, Gianellini L, Croci V, et al. PHA-739358, a potent inhibitor of Aurora kinases with a selective target inhibition profile relevant to cancer. Mol Cancer Ther 2007;6:3158–68.
[18] Krieger E, Vriend G. Model@Home: distributed computing in bioinformatics using a screensaver based approach. Bioinformatics 2002;18:315–8.
[19] Goodsell DS, Morris GM, Olson AJ. Automated docking of flexible ligands: applications of autodock. J Mol Recognit 1996;9:1–5.
[20] Kleywegt GJ. Separating model optimization and model validation in statistical cross-validation as applied to crystallography. Acta Crystallogr 2007;63: 94–100.
[21] Modugno M, Casale E, Soncini C, Rosettani P, Colombo R, Lupi R, et al. Crystal structure of the T315I Abl mutant in complex with the aurora kinases inhibitor PHA-739358. Cancer Res 2007;67:7987–90.
[22] Zhao B, Smallwood A, Yang J, Koretke K, Nurse K, Calamari A, Kirkpatrick RB, Lai Z. Modulation of kinase-inhibitor interactions by auxiliary protein binding: crystallography studies on Aurora A interactions with VX-680 and with TPX2. Protein Sci 2008;17:1791–7.
[23] Stewart JJ. Special issue – MOPAC – A Semiempirical molecular-orbital program. J Comput Aided Mol Des 1990;4:1–45.
[24] Dong JS, Porter TD. Coexpression of mammalian cytochrome P450 and reductase in *Escherichia coli*. Arch Biochem Biophys 1996;327:254–9.
[25] Sadeghi SJ, Meirinhos R, Catucci G, Dodhia VR, Di Nardo G, Gilardi G. Direct electrochemistry of drug metabolizing human flavin-containing monooxygenase: electrochemical turnover of benzydamine and tamoxifen. J Am Chem Soc 2010;132:458–9.
[26] Wagner MA, Khanna P, Jorns MS. Structure of the flavocoenzyme of two homologous amine oxidases: monomeric sarcosine oxidase and N-methyltryptophan oxidase. Biochemistry 1999;38:5588–95.
[27] Perez-Iratxeta C, Andrade-Navarro MA. K2D2: estimation of protein secondary structure from circular dichroism spectra. BMC Struct Biol 2008;8:25–9.
[28] Dixit A, Roche TE. Spectrophotometric assay of the flavin-containing monooxygenase and changes in its activity in femalew mouse liver with nutritional and diurnal conditions. Arch Biochem Biophys 1984;233:50–63.
[29] Motika MS, Zhang J, Zheng X, Riedler K, Cashman JR. Novel variants of the human flavin-containing monooxygenase 3 (FMO3) gene associated with trimethylaminuria. Mol Genet Metab 2009;97:128–35.
[30] Yeung CK, Adman ET, Rettie AE. Functional characterization of genetic variants of human FMO3 associated with trimethylaminuria. Arch Biochem Biophys 2007;464:251–9.
[31] Hamman MA, Haehner-Daniels BD, Wrighton SA, Rettie AE, Hall SD. Stereoselective sulfoxidation of sulindac sulfide by flavin-containing monooxygenases – comparison of human liver and kidney microsomes and mammalian enzymes. Biochem Pharmacol 2000;60:7–17.
[32] Richter RP, Bérat R, Brisson AR. Formation of solid-supported lipid bilayers: an integrated view. Langmuir 2006;22:3497–505.
[33] Dodd CE, Johnson BR, Jeuken LJ, Bugg TD, Bushby RJ, Evans SD. Native *E. coli* inner membrane incorporation in solid-supported lipid bilayer membranes. Biointerphases 2008;3:FA59–67.
[34] Lang DH, Rettie AEJ. In vitro evaluation of potential in vivo probes for human flavin-containing monooxygenase (FMO): metabolism of benzydamine and caffeine by FMO and P450 isoforms. British J Clin Pharmacol 2000;50:311–4.
[35] Stormer E, Roots I, Brockmoller J. Benzydamine N-oxidation as an index reaction reflecting FMO activity in human liver microsomes and impact of FMO3 polymorphisms on enzyme activity. British J Clin Pharmacol 2000;50(6):553–61.
[36] Shimizu M, Yano H, Nagashima S, Murayama N, Zhang J, Cashman JR, Yamazaki H. Effect of genetic variants of the human flavin-containing monooxygenase 3 on N- and S-oxygenation activities. Drug Metab Dispos 2007;35(3):328–30.
[37] Ballard JE, Prueksaritanont T, Tang C. Hepatic metabolism of MK-0457, a potent Aurora kinase inhibitor: interspecies comparison and role of human cytochrome P450 and flavin-containing monooxygenase. Drug Metab Dispos 2007;35:1447–51.
[38] Cohen RB, Jones SF, Aggarwal C, von Mehren M, Cheng J, Spigel DR, et al. A phase I dose-escalation study of Danusertib (PHA-739358) administered as a 24-hr infusion with and without granulocyte colony-stimulating factor in a 14-day cycle in patients with advanced solid tumors. Clin Cancer Res 2009;15(21):6694–701.
[39] Alfieri A, Malito E, Orru R, Fraaije MW, Mattevi A. Revealing the moonlighting role of NADP in the structure of a flavin-containing monooxygenase. Proc Natl Acad Sci USA 2008;105:6572–7.
[40] Eswaramoorthy S, Bonanno JB, Burley SK, Swaminathan S. Mechanism of action of a flavin-containing monooxygenase. Proc Natl Acad Sci USA 2006;103: 9832–7.
[41] Malito E, Alfieri A, Fraaije MW, Mattevi A. Proc Natl Acad Sci USA 2004;101: 13157–62.
[42] Orville AM, Lountos GT, Finnegan S, Gadda G, Prabhakar R. Crystallographic, spectroscopic, and computational analysis of a flavin c4a-oxygen adduct in choline oxidase. Biochemistry 2009;48:720–8.